Journal of Geophysical Research: Oceans

RESEARCH ARTICLE
10.1029/2018JC013825

Special Section:
Forum for Arctic Modeling and Observational Synthesis (FAMOS) 2: Beaufort Gyre phenomenon

Transport of Pacific Water Into the Canada Basin and the Formation of the Chukchi Slope Current

Michael A. Spall[1], Robert S. Pickart[1], Min Li[1,2,3,4], Motoyo Itoh[5], Peigen Lin[1], Takashi Kikuchi[5], and Yiquan Qi[6]

[1]Woods Hole Oceanographic Institution, Woods Hole, MA, USA, [2]State Key Laboratory of Tropical Oceanography, South China Sea Institute of Oceanology, Chinese Academy of Sciences, Guangzhou, China, [3]Guangdong Province Key Laboratory for Coastal Ocean Variation and Disaster Prediction, Guangdong Ocean University, Zhanjiang, China, [4]University of Chinese Academy of Sciences, Beijing, China, [5]Japan Agency for Marine-Earth Science and Technology, Yokosuka, Japan, [6]College of Oceanography, Hohai University, Nanjing, China

Abstract A high-resolution regional ocean model together with moored hydrographic and velocity measurements is used to identify the pathways and mechanisms by which Pacific water, modified over the Chukchi shelf, crosses the shelf break into the Canada Basin. Most of the Pacific water flowing into the Arctic Ocean through Bering Strait enters the Canada Basin through Barrow Canyon. Strong advection allows the water to cross the shelf break and exit the shelf. Wind forcing plays little role in this process. Some of the outflowing water from Barrow Canyon flows to the east into the Beaufort Sea; however, approximately 0.4 to 0.5 Sv turns to the west forming the newly identified Chukchi Slope Current. This transport occurs at all times of year, channeling both summer and winter waters from the shelf to the Canada Basin. The model indicates that approximately 75% of this water was exposed to the mixed layer within the Chukchi Sea, while the remaining 25% was able to cross the shelf during the stratified summer before convection commences in late fall. We view the $\mathcal{O}(0.5)$ Sv of the Chukchi Slope Current as replacing Beaufort Gyre water that would have come from the east in the absence of the cross-topography flow in Barrow Canyon. The weak eastward flow on the Beaufort slope is also consistent with the local disruption of the Beaufort Gyre by the Barrow Canyon outflow.

Plain Language Summary Using a combination of numerical models and field observations, we elucidate where and when waters of Pacific Ocean origin cross the shelf break and enter the interior of the Canada Basin. Most of these waters flow toward the west, forming the recently observed Chukchi Slope Current.

Key Points:
- Westward flow of Pacific origin waters is observed off the shelf break north of the Chukchi Sea
- A regional numerical model traces these waters to the outflow of Barrow Canyon
- This nonlinear advection dominates the cross-isobath flow and supply of Pacific origin waters to the Canada Basin

Correspondence to:
M. A. Spall,
mspall@whoi.edu

Citation:
Spall, M., Pickart, R., Li, M., Itoh, M., Lin, P., Kikuchi, T., & Qi, Y. (2018). Transport of Pacific water into the Canada Basin and the formation of the Chukchi Slope Current. *Journal of Geophysical Research: Oceans*, *123*, 7453–7471. https://doi.org/10.1029/2018JC013825

Received 24 JAN 2018
Accepted 12 SEP 2018
Accepted article online 2 OCT 2018
Published online 22 OCT 2018

©2018. American Geophysical Union. All Rights Reserved.

1. Introduction

Pacific origin water strongly influences the hydrographic structure of the western Arctic Ocean and plays a critical role in the functioning of the regional ecosystem. The upper halocline of the Canada Basin contains warm Pacific summer water atop cold Pacific winter water, which together dictate the stratification that sheilds the underlying warm Atlantic layer from the pack ice. The cold Pacific water also supplies the basin with nutrients (Codispoti et al., 2005) as well as carbon (Mathis et al., 2007), the latter of which is now contributing to enhanced levels of ocean acidification (Cross et al., 2017). Zooplankton and other organisms are fluxed into the Canada Basin with the warm Pacific water (Ashjian et al., 2010; Hopcroft et al., 2010; Nelson et al., 2009), which in turn influences the feeding patterns of upper trophic species (Wassmann et al., 2015). The warmest summer water also represents a significant source of freshwater to the western Arctic (Woodgate et al., 2012) which is accumulated in the Beaufort Gyre (Proshutinsky et al., 2009). Despite these and other known impacts of Pacific water, there remains considerable uncertainty as to how and where the water is transported from the shelves into the interior. A better understanding of this shelf-basin transfer of mass and properties is thus required, not only to enhance our knowledge of the western Arctic ecosystem but to be able to predict how it might change in response to a warming climate.

Over the years a number of observational and modeling studies have sharpened our view of the circulation and modification of Pacific water as it progresses across the Chukchi shelf. To first order, there are three main

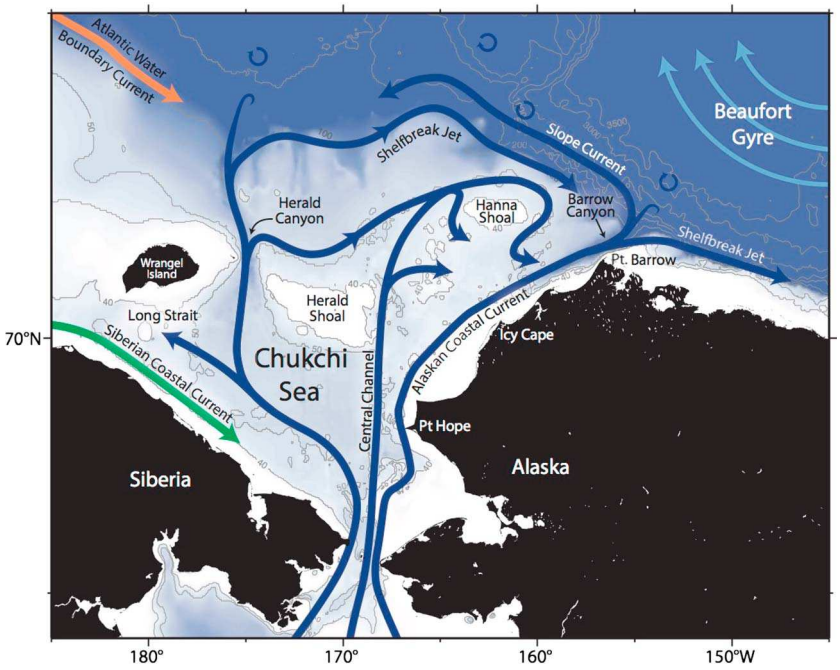

Figure 1. Schematic circulation of the Chukchi Sea and place names, after Corlett and Pickart (2017).

flow branches, largely dictated by the topography of the shelf: the coastal branch (known in summertime as the Alaskan Coastal Current; e.g., Paquette & Bourke, 1974), the Central Channel branch (e.g., Weingartner et al., 2005), and the western branch that flows through Herald Canyon (Pickart et al., 2010; Woodgate et al., 2005b; see Figure 1). Numerical models generally support this view, although they indicate that the shelf circulation is highly sensitive to synoptic wind forcing (Panteleev et al., 2010; Spall, 2007; Winsor & Chapman, 2004). For example, the flow in all three branches can be reversed to the south under northerly winds (Pickart et al., 2010, 2011; Weingartner et al., 2017), as can the flow through Bering Strait (Woodgate et al., 2005a). Recently, it has been demonstrated that these flow branches interact with each other to some degree. For example, part of the western branch north of Herald Canyon is diverted to the central branch, which subsequently splits into smaller filaments that converge with the coastal branch as the water enters Barrow Canyon (see Figure 1).

Despite our improving understanding of the circulation of the Chukchi Sea, the manner and location in which the Pacific water subsequently exits the shelf into the basin is still far from clear. This is complicated by the topography of the Chukchi Sea, in which the definition of what is the shelf and what is the basin interior is ambiguous. For example, the depth at which the shelf break occurs varies by as much as 100 m (B. Corlett, personal communication, 2017). Using sparsely positioned moorings spanning the Chukchi Sea, Woodgate et al. (2005b) argued that, averaged over the year, roughly equal amounts of Pacific water leave the shelf through Long Strait, Herald Canyon, and Barrow Canyon. If or where these waters enter the basin (versus remaining on the outer shelf) is not known. During the summer months it appears that the majority of the Pacific water can at times flow through Barrow Canyon (Gong & Pickart, 2015; Itoh et al., 2013; Pickart et al., 2016). Part of the uncertainty is due to the fact that, to date, there have been no high-resolution mooring arrays deployed in Long Strait or Herald Canyon; hence, we have no robust observational estimates of the transport through these geographical constrictions. Moreover, the mooring arrays deployed within and near Barrow Canyon have provided differing results. For example, Itoh et al. (2013) report a yearly mean Pacific water transport of 0.44 Sv at the mouth of the canyon, while Weingartner et al. (2017) estimate a mean value of only 0.20 Sv at the head of the canyon. This discrepancy could be due in part to instrument coverage. The climatological transport through Bering Strait is of $\mathcal{O}$(0.8 Sv) (Woodgate et al., 2005a), although this has recently increased to an annual mean value of 1.1 Sv (Woodgate, 2017).

It is possible that there is a net flux of Pacific water across the Chukchi shelf break due to turbulent or wind-driven processes. It is now well established that, in the absence of wind, there is an eastward flowing

current along the shelf break of the Chukchi Sea (Corlett & Pickart, 2017; Li & Pickart, 2017; Watanabe et al., 2017). The jet is baroclinically unstable and can spawn both cold-core and warm-core eddies of Pacific water (Mathis et al., 2007; Pickart et al., 2005; Pickart & Stossmeister, 2009). We note that the numerical model study of Spall et al. (2008) suggests that, while this process fluxes tracers off-shelf, there is no net mass flux; that is, it is an exchange of water. On the other hand, Timmermans et al. (2017) argue that Pacific water is subducted from the mixed layer on the Chukchi shelf to the halocline of the Canada Basin by wind forcing via a combination of lateral induction and Ekman pumping. Using a numerical model, they estimate that this results in net flux of 0.4 Sv across the Chukchi shelf break, which is the same magnitude that Itoh et al. (2013) estimate flows out of Barrow Canyon.

Recently, Corlett and Pickart (2017) have documented the existence of a westward flowing current along the continental slope of the Chukchi Sea — seaward of the shelf break jet — which they named the Chukchi Slope Current. Using 46 shipboard crossings of the current occupied over a period of 12 years, Corlett and Pickart (2017) estimate that it transports 0.5 Sv of Pacific water. They argue that the $\mathcal{O}$(50 km) wide slope current emanates from the outflow from Barrow Canyon, which is consistent with the shipboard measurements discussed in Brugler et al. (2014) and the surface drifter trajectories presented in Weingartner et al. (2015) and Stabeno et al. (2018). While the shipboard data used by Corlett and Pickart (2017) were collected exclusively during the summer months, a mooring array deployed west of Barrow Canyon has confirmed that the Chukchi Slope Current is a year-round feature Li and Pickart (2017).

In summer the current is surface intensified, and during the cold months of the year it is middepth-intensified (averaged over the year it is surface intensified). This latter observation is consistent with the modeling results of Watanabe et al. (2017). By taking into account the Chukchi Slope Current, Corlett and Pickart (2017) were able to construct a balanced mass budget of the inflows/outflows of the Chukchi shelf. This seems to be at odds with the large off-shelf subduction of Pacific water that Timmermans et al. (2017) calculate. It should be noted, however, that the model employed by Timmermans et al. (2017) is coarse (36-km lateral resolution) and thus incapable of resolving either the Chukchi shelf break jet or the Chukchi Slope Current.

In the interior Canada Basin the circulation is dominated by the Beaufort Gyre, which is driven by the anticyclonic wind stress curl associated with the Beaufort High (Moore, 2012). The gyre varies in size and strength on seasonal time scales (Proshutinsky et al., 2002) as well as interannually (Proshutinsky et al., 2009). Over the past decade the freshwater content of the gyre has significantly increased due to an extended period of anticyclonic atmospheric forcing (Proshutinsky et al., 2015). Using satellite measurements of sea surface height, Mizobata et al. (2016) demonstrated that the gyre varies from month to month, yet the surface speeds of the gyre generally remain on the order of 10 cm/s. Using their calculated velocity fields, Mizobata et al. (2016) investigated the fate of Pacific water in the Canada Basin by releasing a passive tracer in the vicinity of Barrow Canyon for different years. The tracer was consistently advected to the west and then north by the gyre, although in some years much of it remained close to the shelf break of the Chukchi and East Siberian Seas. However, no mention was made of a slope current over the continental slope. Watanabe et al. (2017) did a similar tracer release in their model and also found that a large proportion of the Pacific water emanating from Barrow traveled to the west. They noted that this pathway was distinct from the southern arm of the Beaufort Gyre and referred to it as a shelf break flow. Considering the observations of Corlett and Pickart (2017) and Li and Pickart (2017), it is clear that the Watanabe et al. (2017) westward pathway is the Chukchi Slope Current. A similar anticyclonic circulation was found for water originating on the shelf in a model by Timmermans et al. (2014), although the resolution of the model was likely not sufficient to distinguish the Chukchi Slope Current from the Beaufort Gyre.

In light of these recent studies, numerous questions arise regarding the circulation north of the Chukchi Sea and the fate of the Pacific water emanating from the shelf. For instance, does a sizable portion of the outflow from Barrow Canyon turn west to form the Chukchi Slope Current? If so, what are the dynamics that govern this? Also, what is the fate of the Pacific water advected by the current and how does it enter the basin? What are the relative contributions to the source waters of the Canada Basin halocline from the advective outflow from Barrow Canyon versus subduction from the mixed layer of the Chukchi Sea across the shelf break to the west of Barrow Canyon? Finally, how is the Chukchi Slope Current related to the southern portion of the Beaufort Gyre? In this study we address some of these questions.

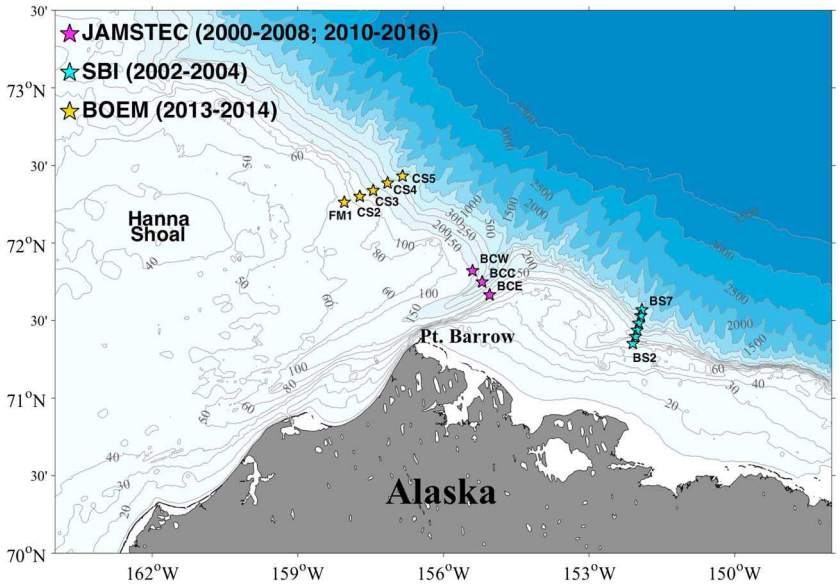

Figure 2. Locations of the three mooring arrays whose data are used in the study. See the legend for the time periods of the measurements. JAMSTEC = Japan Agency for Marine-Earth Science and Technology; SBI = Western Arctic Shelf-Basin Interactions Program; BOEM = Bureau of Ocean Energy and Management.

2. Methods

A regional numerical model and mooring observations are used to describe the circulation in the vicinity of the Chukchi shelf break, Barrow Canyon, and the southern Beaufort Gyre. The observations are used to identify the currents, document transports, and infer pathways based on water mass properties. The numerical model is first evaluated in terms of its ability to reproduce the basic characteristics of the flow observed at key locations and then used to identify the pathways and mechanisms of exchange across the Chukchi shelf break.

2.1. Observational Resources

Time series from three different mooring arrays are used in the study: a high-resolution array that was deployed across the Beaufort Sea shelf/slope, three moorings that have been maintained across the mouth of Barrow Canyon, and an array that spanned from the outer shelf to the upper slope of the Chukchi Sea (Figure 2). The Beaufort array was part of the Western Arctic Shelf-Basin Interactions program and was in place from August 2002 to September 2004. This consisted of seven moorings spanning from the outer shelf to the midcontinental slope. The inner five moorings contained coastal moored profilers providing vertical traces of temperature and salinity four times daily at 2-m resolution. The profiles extended only to 50-m depth, since it was deemed unsafe to have the mooring top floats be any shallower than this due to the risk of ridging pack ice. Velocity at these sites was measured using upward facing acoustic Doppler current profilers (ADCPs) near the bases of the moorings. These provided vertical traces of eastward and northward currents at 5- to 10-m resolution every hour. The two offshore moorings contained McLane moored profilers sampling twice per day. The velocity at these sites was measured by a travel time acoustic current meter on the profiler. The resolution of both the hydrographic and velocity profiles was 2 m. The velocity data from all of the moorings were detided using the T-TIDE harmonic analysis toolbox (Pawlowicz et al., 2002). The reader is referred to Spall et al. (2008), Nikolopoulos et al. (2009), and Li and Pickart (2017) for details regarding data coverage, the processing of the data, and the accuracy of the measurements.

More recently, a single mooring near the shelf break (mooring BS3, Figure 2) has been maintained since 2008 as part of the Arctic Observing Network. This was configured similarly to the original mooring at the site, but in recent years the profiler has been replaced by discrete MicroCATs. Also, in some years two ADCPs have been used, one near the bottom and a second upward facing instrument on the top float. Further details regarding the Arctic Observing Network mooring can be found in Brugler et al. (2014) and Lin et al. (2018). The transport of the boundary current is estimated for these years using a proxy that was developed by Brugler et al. (2014) and shown to be highly accurate.

The moorings in Barrow Canyon are maintained by the Japan Agency for Marine-Earth Science and Technology and have been in place (with some interruptions) since 1999. The moorings are spaced 10 km apart and contain MicroCATs for measuring pressure, temperature, and salinity and a combination of point current meters and ADCPs for velocity. The uppermost MicroCATs are situated near 30-m depth. The data are interpolated onto a regular grid and low-passed using a 25-hr filter width. Itoh et al. (2013) provide details on the data configuration, processing, and accuracy of the sensors.

The mooring array spanning the Chukchi shelf break and upper slope was deployed as part of a program entitled *Characterization of the Circulation on the Continental Shelf Areas of the Northeast Chukchi and Western Beaufort Seas*. The array was composed of five moorings deployed from October 2013 to September 2014. Each of the moorings contained a coastal moored profiler providing vertical traces of temperature and salinity at 2-m resolution four times per day and an upward facing ADCP providing hourly vertical profiles of velocity. The top floats of the moorings were situated at 35-m depth. All of the velocity data were detided in the same way as for the Beaufort slope mooring data. Details concerning the instrumentation and the data are given in Li and Pickart (2017). At all of the array sites we defined Pacific water as fresher than 34, following Itoh et al. (2013). We also use climatological data from the Bering Strait mooring array published in Woodgate et al. (2005a).

2.2. Model Configuration and Forcing

A regional version of the Massachusetts Institute of Technology general circulation model (MITgcm; Marshall et al., 1997) is set up for the Chukchi Sea and Canada Basin. It solves the hydrostatic, primitive equations of motion on a staggered Cartesian C-grid at fixed depth levels. The partial cell treatment of bottom topography allows for accurate representation of steep topography in the presence of stratification, expected to be important for the exchange of properties across the shelf break.

The model is coupled to a thermodynamic/dynamic sea ice model. (Details can be found at http://mitgcm.org/public/r2_manual/latest/online_documents/node2.html.) The dynamics are elastic-viscous-plastic (Hunke & Dukowicz, 1997). The thermodynamics are modeled with a three-layer scheme that permits heat storage in ice (Semtner, 1976), as reformulated by Winton (2000). The albedo reflects that of wet (0.66) or dry (0.75) ice, depending on if there is sufficient heat flux to form melt ponds. The model represents two layers of ice (the upper layer has variable heat capacity resulting from brine pockets) and an overlying layer of snow. The model produces ice thickness and concentration.

The domain is set on an f plane with the Coriolis parameter constant at $f_0 = 1.2 \times 10^{-4}$ s^{-1}. The model is configured on a 1,465-km by 2,158-km Cartesian grid with the southwest corner at 63°N and 180°W. The western boundary of the model domain follows the 180° meridian, while the southern boundary follows the 63°N latitude circle. The grid spacing is variable, ranging from 2 km in the vicinity of Barrow Canyon to 5 km over the Chukchi Sea and southern Canada Basin, to 11 km on the offshore side of the Beaufort Gyre (Figure 3). The bottom topography is interpolated from the ETOPOv2 global topography on a 2-min grid to the model grid. The maximum depth in the model is 1,000 m. The vertical grid spacing is 5 m over the upper 80-m depth, gradually increasing to 50 m at 250-m depth and further increasing to 200 m between 800 and 1,000 m. There is also a channel connecting the eastern shelf with the inflow at Bering Strait. A similar configuration of the model was used by Spall (2007) in a lower-resolution study of the circulation in the Chukchi Sea. The model is regional and has artificial boundaries away from the coast. While we are encouraged by the favorable comparisons between the model and observations, both here and in Spall (2007), we recognize that the presence of these boundaries may be having some influence on the circulation over the Chukchi shelf and in the vicinity of the shelf break.

Subgridscale horizontal viscosity A is parameterized by the Smagorinsky (1963) deformation-dependent scheme as

$$A = \left(\frac{\nu\delta}{\pi}\right)^2 D, \qquad D = [(u_x - v_y)^2 + (u_y + v_x)^2]^{1/2}, \tag{1}$$

where δ is the model grid spacing, $\nu = 2.5$ is a nondimensional coefficient, D is the deformation field, and subscripts indicate partial differentiation. Vertical viscosity and diffusivity are represented with the K_Profile Parameterization (KPP) mixing parameterization (Large et al., 1994) and background mixing coefficients of 10^{-5} m^2/s. There is also a quadratic bottom drag with coefficient 2×10^{-3}. The lateral boundary conditions are no-slip and no normal flux. The model utilizes the nonlinear equation of state of Jackett and McDougall (1995).

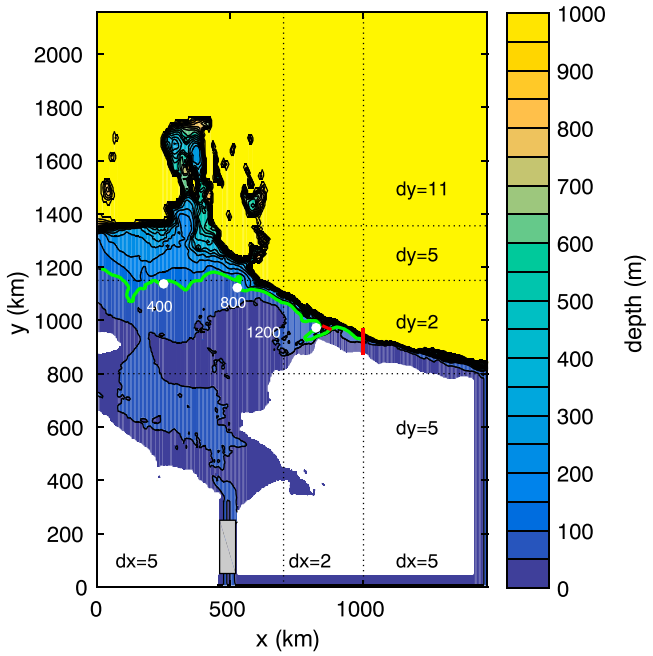

Figure 3. The model domain and bottom topography. The grid spacing is variable, as indicated on the figure with transitions marked by the dotted lines. The gray box near $x = 500$ km, $y = 200$ km is the region of restoring terms forcing the flow through Bering Strait. The two red lines mark the locations of the sections shown in Figures 5 and 6. The bold green line indicates the 100-m isobath, and the white dots indicate distance along that isobath from the western boundary of the model, plotted in Figure 8.

The model is initialized with temperature and salinity interpolated from the PHC3.0 January climatology, updated from Steele et al. (2001). North of $y = 1{,}250$ km and at depths below 35 m the temperature and salinity in the model are restored toward this climatology with a time scale of 2.5×10^6 s. This helps to maintain the anticyclonic Beaufort Gyre circulation in the presence of the model solid boundaries in the basin interior. The fields in the Chukchi Sea, in the vicinity of Barrow Canyon and the shelf break, and in the seasonal mixed layer in the Beaufort Gyre, are freely evolving; there are no artificial restoring terms.

The model is forced by surface fluxes of heat, fresh water, and momentum derived from the monthly mean North American Regional Reanalysis model output (32-km grid, averaged between years 1979 and 2000, http://www.esrl.noaa.gov/psd/data/gridded/data.narr.html). The sensible and latent heat fluxes are derived from 10-m atmospheric winds, 2-m atmospheric temperature, and specific humidity using the bulk formulae of Large and Pond (1981). The downward longwave and shortwave radiation are also specified, while the outgoing longwave radiation is calculated from the surface temperature. The surface momentum flux is derived from atmospheric winds.

The model is also forced by transport through Bering Strait. The volume flux, temperature, and salinity of the inflowing water are based on long-term measurements in the strait (Weingartner et al., 2005; Woodgate et al., 2005a), as in Spall (2007). This is achieved by strongly restoring the model temperature, salinity, and meridional velocity toward prescribed values within the gray box in Bering Strait in Figure 3. The hydrographic properties and transport of the inflow vary with season, with cold, salty water in winter and warm, fresh water in summer and fall; details can be found in the above references.

The central model was run for 2 years with repeat monthly mean atmospheric forcing. Several sensitivity calculations were also carried out (see Table 1). In one, no-inflow, the Bering Strait is closed and all other forcing is the same as the central case, while in another calculation (no-atmos) the forcing in Bering Strait is the same but all atmospheric forcing and sea ice are eliminated. This pair of calculations is used to help understand the forcing mechanism for the Chukchi Slope Current and to distinguish it from the Beaufort Gyre. A final calculation in which all forcing was the same except the velocity toward which the model is restored in Bering Strait and the winds were set to the annual mean (seasonal T/S) is used to demonstrate that the seasonal

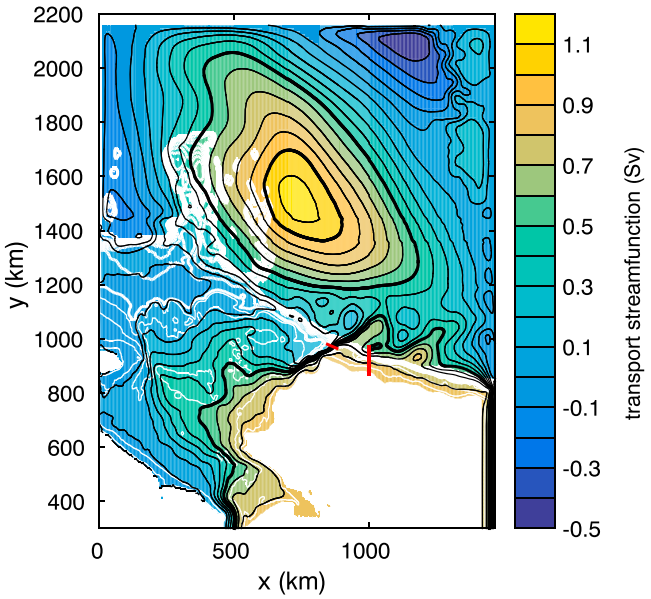

Figure 4. Mean transport stream function calculated down to 300-m depth over the 2 years of model integration (black contours). Bold contours mark the 0.5- and 1.0-Sv levels. White contours are the bottom topography down to 1,000 m; contour interval is 20 m for depths less than 100 m (thin lines) and 100 m between 100 and 1,000 m (bold lines). The red lines indicate the locations of the sections shown in Figures 5 and 6.

cycle in Chukchi Slope Current transport is related to the seasonal cycle in stratification, not transport through Bering Strait.

3. Mean Circulation

The mean model transport stream function in the upper 300 m is shown in Figure 4 along with the bottom topography. The mean transport through Bering Strait is 0.81 Sv, consistent with the long-term measurements of Woodgate et al. (2005a). The flow over the Chukchi shelf is in line with observational estimates Woodgate et al. (2005b) and the previous model of Spall (2007). In particular, there are three primary pathways: through Herald Canyon, through the Central Channel, and along the Alaskan coast. Most of this transport follows the topography and turns toward the east along the outer shelf, converging at the head of Barrow Canyon. Due to the convergence of topographic contours, there is very rapid flow through the canyon.

Of the approximately 0.8 Sv of transport flowing into Barrow Canyon, 0.6 Sv flows into basin and 0.2 Sv remains on the shelf and flows to the east. Of the transport going into the basin interior, approximately 0.4 Sv turns to the west and 0.2 Sv turns to the east. This result supports the argument made by Corlett and Pickart (2017) that the westward flowing Chukchi Slope Current emanates from Barrow Canyon. It is also consistent with surface drifter studies (Stabeno et al., 2018; Weingartner et al., 2015) as well as with the numerical results of Watanabe et al. (2017) who focused on the circulation during the winter months. To the north of the Chukchi Sea, the Beaufort Gyre spans most of the deep basin in the model, with a transport of just over 1 Sv. Note that this circulation and hydrography for *y* greater than 1,250 km is largely constrained by the PHC3.0 climatology to which the model hydrography is restored. The shape of the model Beaufort Gyre on this cartesian grid

Table 1
Summary of Model Calculations

Run	Bering Strait velocity	Bering Strait T and S	Atmospheric buoyancy	Atmospheric wind	Sea ice
central	seasonal	seasonal	seasonal	seasonal	yes
no-inflow	closed	closed	seasonal	seasonal	yes
no-atmos	seasonal	seasonal	none	none	no
seasonal *T/S*	ann mean	seasonal	seasonal	ann mean	yes

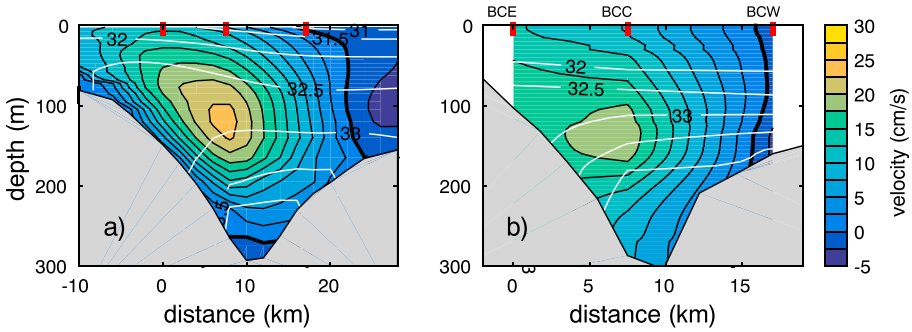

Figure 5. Section of the 2-year mean (a) normal velocity and salinity (white contours, contour interval 0.5) from the model in Barrow Canyon (see location in Figure 4). Positive velocities are down-canyon (to the northeast). The viewer is looking up-canyon (to the southwest). (b) Climatological mean along-canyon velocity and salinity (white contours, contour interval 0.5) at the mouth of Barrow Canyon measured by the Japan Agency for Marine-Earth Science and Technology mooring array. The locations of the moorings are indicated by the red tick marks at the top of each figure. BCE = Barrow Canyon East mooring; BCC = Barrow Canyon Central mooring; BCW = Barrow Canyon West mooring. See Figure 2.

looks different from the usual polar projection but is consistent with this climatological hydrography. South of this restoring region and east of Barrow Canyon (within about 200 km of the north slope of Alaska) there is a weak, meandering flow toward the east, transporting water that originated from Barrow Canyon. This fluid, plus that which turned west at Barrow Canyon, ultimately closes the circulation to the south in the channel along the eastern boundary, to be returned to the Chukchi Sea through Bering Strait.

Our focus is on the sources of Pacific water that cross the shelf break at Barrow Canyon and turn westward. However, before addressing this we first discuss the flow through the canyon and the portion of it that turns to the east on the shelf, as these components of the circulation are reasonably well established in the observational literature. The mean velocity and salinity in the model within Barrow Canyon (the western bold red line in Figure 4) are shown in Figure 5a. The flow through the canyon has a middepth maximum and is banked up against the southeastern side. The maximum zonal velocity is about 22 cm/s. The water is weakly stratified at middepth over the eastern flank of the canyon. The climatological mean along-canyon velocity measured by the Japan Agency for Marine-Earth Science and Technology array is also characterized by a middepth maximum (roughly 17 cm/s), with the strongest flow on the eastern flank of the canyon (Figure 5b). As is the case in the model, the eastern flank has weaker stratification than off-shelf (recall that the mooring data do not extend above 30-m depth).

To the east of Barrow Canyon, the mean zonal velocity in the model (the eastern bold red line in Figure 4) is shown in Figure 6a. The zonal flow has a subsurface maximum of about 8 cm/s centered just off the shelf break. The mean current is fairly narrow, about 20 km wide, and is concentrated in the upper 200 m. The water in the current has weaker stratification (low potential vorticity) as a result of convectively formed winter water originating on the Chukchi shelf (e.g., Pickart et al., 2005). Such a mean kinematic and water mass structure of

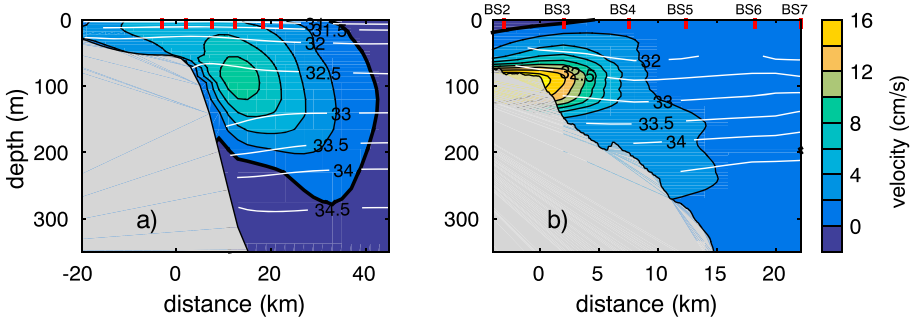

Figure 6. Section of the 2-year mean (a) zonal velocity and salinity from the model at x = 1,000 km (the approximate location of the mooring array). (b) Year-long (2002–2003) mean along-stream velocity and salinity near 152°W on the Beaufort slope (see Figure 2 for the location of the array) from Nikolopoulos et al. (2009). Positive velocities are eastward. The locations of the moorings are indicated along the top by the red tick marks. The viewer is looking to the west.

the Beaufort shelf break jet is in line with the observations in Figure 6b (Nikolopoulos et al., 2009), although the observed current is much narrower and faster than that in the model (note that the salinity data from the moorings is limited to depths deeper than 50 m).

4. Flux of Pacific Origin Water Across the Shelf Break

As seen above, the regional model produces currents and transports through the Chukchi Sea, Barrow Canyon, and along the shelf break east of Barrow that are consistent with the observations. We now use the model fields to connect the westward flow seaward of the Chukchi shelf break to the Chukchi Slope Current and the northward transport through Barrow Canyon. For purposes of discussion, we define the Chukchi shelf to extend to the 100-m isobath and the upper slope to lie between the 100-m isobath and the 300-m isobath. Offshore of the 300-m isobath we refer to as the Canada basin interior.

4.1. Chukchi Slope Current

The 46 shipboard sections used by Corlett and Pickart (2017) indicated that the Chukchi Slope Current transports 0.50 Sv of Pacific origin waters toward the west during the summer months, offshore of the shelf break. Using data from the mooring array across the Chukchi shelf break/upper slope (Figure 2), Li and Pickart (2017) estimated a similar value (0.57 Sv) for the annual mean transport. (The mooring array did not capture the offshore edge of the current, so Li & Pickart, 2017, applied an extrapolation technique. Nevertheless, it is likely that their mean transport value is an underestimate.) The presence of Pacific water in the upper halocline of the Canada Basin is well established (e.g., Steele et al., 2004). There have been several mechanisms proposed as a means to transport the Pacific water across the shelf break. Instabilities of the shelf break jet produce small eddies with modified Pacific water in their core (Mathis et al., 2007; Pickart et al., 2005). While commonly observed in the basin interior (Manley & Hunkins, 1985; Zhao et al., 2014), these are distinct from the large-scale westward flow of the Chukchi Slope Current. Previous models of the region have produced an off-shelf flow from Barrow Canyon into the basin interior (Aksenov et al., 2016; Zhang et al., 2016), but these models had lower spatial resolution and did not focus on this shelf-basin exchange. The recent study by Watanabe et al. (2017) used observations and a high-resolution Arctic model to connect a seasonal warming of the halocline in the Chukchi Borderland region to outflow from Barrow Canyon via westward advection by the slope current (which they referred to as a shelf break flow). Timmermans et al. (2017) propose that Pacific water is advected from the Chukchi shelf to the halocline in the interior of the Canada Basin by wind forcing.

The model velocity parallel to the 75-m isobath, averaged over the final 6 months of integration along the shelf between $x = 600$ km and $x = 830$ km, is shown as a function of offshore distance and depth in Figure 7a. We chose the final 6 months in order to show the penetration of a tracer marking Pacific origin water (Figure 7d) and the along-shelf average to avoid aliasing meanders and eddies that are present at any particular section. There is a bottom intensified eastward flow centered near the shelf break (distance less than 30 km) and a surface intensified westward flow just offshore of the shelf break (distance between 30 and 150 km). These correspond with the Chukchi shelf break jet and Chukchi Slope Current, respectively. The westward flow at the offshore part of the section (distance between 150 and 200 km) is the southern arm of the Beaufort Gyre (see below). The model Chukchi Slope Current is salt stratified, while the shelf break jet (which emanates from Herald Canyon) has a weakly stratified core (Figure 7c), indicating low potential vorticity as a result of wintertime convection in the Chukchi Sea. This compares favorably to the summertime mean slope current section of Corlett and Pickart (2017) as well as the year-long mean section of Li and Pickart (2017) constructed using the mooring data (Figure 7b), although the model current is much slower and wider than the observations. As noted above, Li et al.'s (submitted) section does not bracket the entire slope current, but Corlett and Pickart's (2017) section does extend seaward of the current and captures the southern edge of the westward flowing Beaufort Gyre.

4.2. Mean Shelf-Basin Flux

The mean transport perpendicular to the 100-m isobath (see Figure 3 for reference) indicates where the Pacific water exits the shelf. The mean transport over the 2-year integration was calculated relative to the western boundary in the model and integrated downward from the surface along the 100-m isobath (Figure 8). Regions of vertical gradients indicate the depths, and horizonal gradients indicate the along-shelf location, of the flow across the topography. The primary region of exchange is at a distance 1,300 km from the western boundary, the location of Barrow Canyon. It occurs throughout the water column but is most concentrated between 50- and 80-m depth. This is consistent with the subsurface maximum in the mean velocity in Barrow

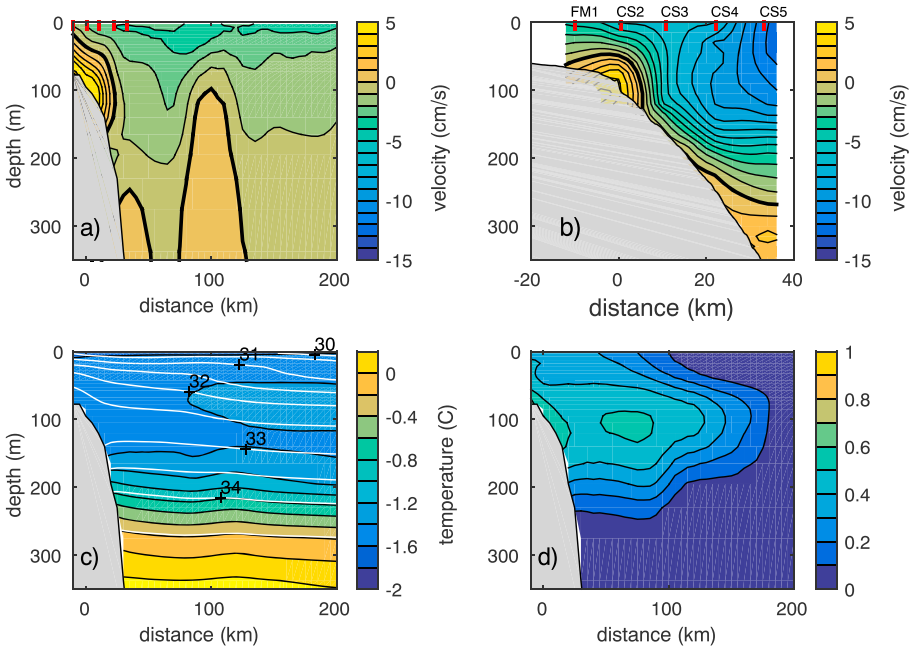

Figure 7. Mean sections between $x = 600$ km and $x = 830$ km for the final 6 months of (a) along-topography velocity (cm/s); (b) year-long (2013–2014) mean along-stream velocity near 157°W on the Chukchi slope (see Figure 2 for the location of the array) from Li and Pickart (2017). The bold black line in (a) and (b) marks the zero contour. (c) Temperature (colors) and salinity (white contours, contour interval 0.5); (d) Pacific water tracer. The offshore distance and along-topography velocity from the model are mapped relative to the 75-m isobath. Positive velocities are eastward. The locations of the moorings are indicated along the top. The viewer is looking to the west.

Canyon. There is a net flux across the 100-m isobath west of Barrow Canyon of about 0.2 Sv. This occurs primarily along the steep slope between $x = 800$ km and the western flank of Barrow Canyon. The off-shelf flux is concentrated near the bottom, suggestive of off-shelf transport in the bottom Ekman layer (related to the eastward shelf-break jet, Figure 7).

The model calculation with no atmospheric forcing or sea ice produces a nearly identical transport across the 100-m isobath, so wind does not appear to be an important factor in off-shelf transport. Ekman pumping along the Chukchi slope west of Barrow Canyon is estimated to be of order $W_E = 20$ m/year, which produces a total of only 0.05 Sv of downward transport (Meneghello et al., 2018), an order of magnitude smaller than the transport in Barrow Canyon. This Ekman pumping would also produce an off-shelf transport analogous to the southward Sverdrup transport in subtropical gyres. The magnitude of this transport can be estimated by a simple linear vorticity balance with $\beta_T V_T = f W_E / H$, where V_T is the cross-isobath velocity, $\beta_T = f\alpha/H$ is the topographic beta, α is the bottom slope, and H is the bottom depth. This simplifies to $V_T = W_E/\alpha$, which gives rise to a transport estimate of $\Psi = W_E L H/\alpha$, where L is the along-shelf length scale over which the Ekman pumping acts. The region of persistent downward Ekman pumping identified by Meneghello et al. (2018) lies along the outer shelf roughly between 160°W to 170°W and 70°N to 72°N. The average bottom slope in this region between the 100- and 200-m isobaths is $\mathcal{O}(0.002)$. A uniform Ekman pumping of $W_E = 20$ m/year results in an off-shelf velocity of $\mathcal{O}(3.5 \times 10^{-4}$ m/s), and taking an along-shelf distance of $L = 400$ km and an average bottom depth of $H = 150$ m gives an off-shelf transport of $\mathcal{O}(0.02$ Sv), more than an order of magnitude less than the cross topography transport in Barrow Canyon. Consideration of a nonzero vertical velocity at the bottom would reduce this transport even further. Even allowing for some shielding of the topographic slope

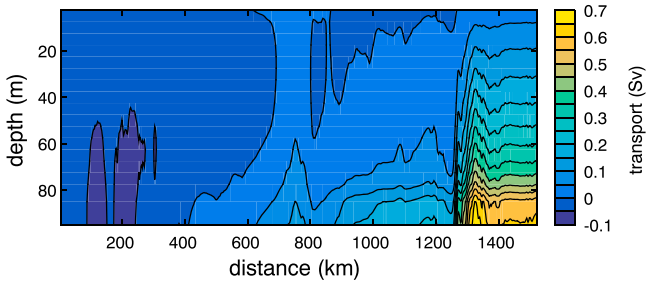

Figure 8. The transport across the 100-m isobath, integrated from surface to bottom and from the western boundary of the domain to $x = 1{,}000$ km (Sv). The bold black line marks the zero contour. This path is indicated in Figure 3 by the bold green line, with distance markers provided for reference.

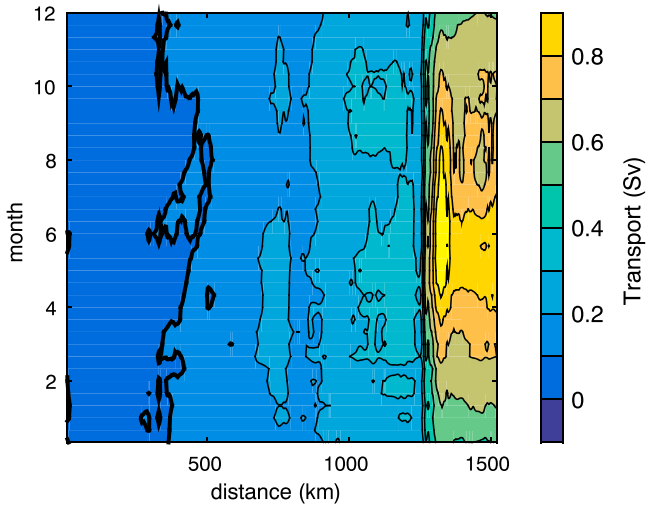

Figure 9. The transport across the 100-m isobath, integrated from surface to bottom as a function of distance from the western boundary of the domain and time. This is the average seasonal cycle based on 2 years of model integration. The 100-m isobath is indicated in Figure 3 by the bold green line, with distance markers provided for reference.

effect due to stratification in summer, it is unlikely that this can account for significant cross topography transport.

4.3. Seasonality

It is well known that there is a strong seasonal cycle in the water mass properties in the Chukchi Sea and in the transport through Bering Strait (Woodgate et al., 2005a; 2005b). The depth-integrated transport across the 100-m isobath as a function of month (averaged between the 2 years to reduce internal variability) and along-shelf distance shows that, while the magnitude of the transport across the topography changes with season, the location does not (Figure 9). Analysis as a function of depth also shows little seasonality.

The transport across the 100-m isobath as a function of month and salinity is shown in Figure 10. The salinity generally falls between 32 and 34, although there are weaker fluxes with lower salinity in summer and fall. The winter and early spring flux spans a wide range of salinities, while the late summer and fall salinity is more concentrated around 32.8. There is a negative salinity flux around 32 during January and February. This is a signature of an eddy-driven exchange, with higher-salinity water moving offshore and lower-salinity water moving onshore. There is no corresponding onshore net transport across this isobath (Figure 9).

The mean transport stream function shows that the off-shelf flow from Barrow Canyon splits just seaward of the canyon—part of it turning toward the west and part toward the east (Figure 4). A time series of the model transport at Barrow Canyon, through Bering Strait, and westward across $x = 800$ km between $y = 1{,}000$ km (depth = 116 m) and $y = 1{,}250$ km (which is indicative of the Chukchi Slope Current) is shown in Figure 11a. This is an annual cycle taken as the average of the 2 years in the model integration. Each year is similar, but we present an average to reduce some of the internal variability. The bold dashed line is for the case with no seasonal cycle in restoring velocity at Bering Strait and no seasonal cycle in wind-forcing but includes the seasonal cycle in the inflowing temperature and salinity at Bering Strait and in the atmospheric temperature and downward longwave and shortwave radiation (model run seasonal *T*/*S*).

The model transport through Bering Strait is a minimum in winter at about 0.6 Sv and a maximum in summer at about 1.1 Sv. The transport through Barrow Canyon (dash-dotted line) shows a very similar seasonal cycle. It peaks roughly 2 weeks after Bering Strait with almost 0.2 Sv less transport. This is the amount lost from the shelf to the west of Barrow Canyon (Figure 8). The westward transport in the Chukchi Slope Current shows a peak in late summer and fall, about 2–3 months later than the peak transport in Barrow Canyon. It is also more steady in winter and spring, while the Bering Strait and Barrow Canyon transports vary more sinusoidally year round.

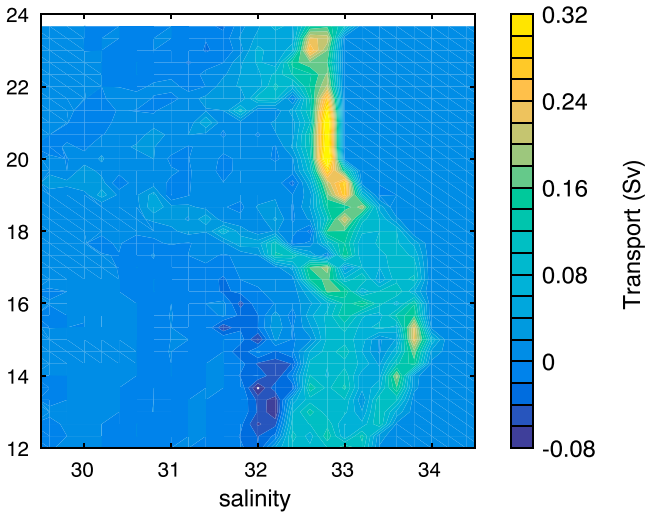

Figure 10. The transport across the 100-m isobath, between the model western boundary and $x = 1{,}000$ km as a function of salinity (0.2-ppt increments) and time. This is calculated over the second year of integration only. The 100-m isobath is indicated in Figure 3 by the bold green line.

Why is there a difference in the timing of the peak transport of the slope current versus the Barrow Canyon ouflow? One possibility is the influence of stratification. The thin dashed line in Figure 11a shows the change in density in the model from top to bottom in Barrow Canyon. It is weakly stratified most of the year but has increased stratification roughly between months 5 and 9. This corresponds well to the period of enhanced westward transport of the slope current. During months 1 through 5 the transport through Barrow Canyon is increasing while the westward transport offshore is fairly steady, so the increase in westward transport in late summer is not simply a reflection of enhanced transport in Barrow Canyon. The transport across the topography follows the seasonal cycle in Barrow Canyon (Figure 9), so this change in westward transport is an indication of a change in the direction of the offshore flow from stronger to the east in winter/spring to stronger to the west in summer/fall. A hueristic explana-

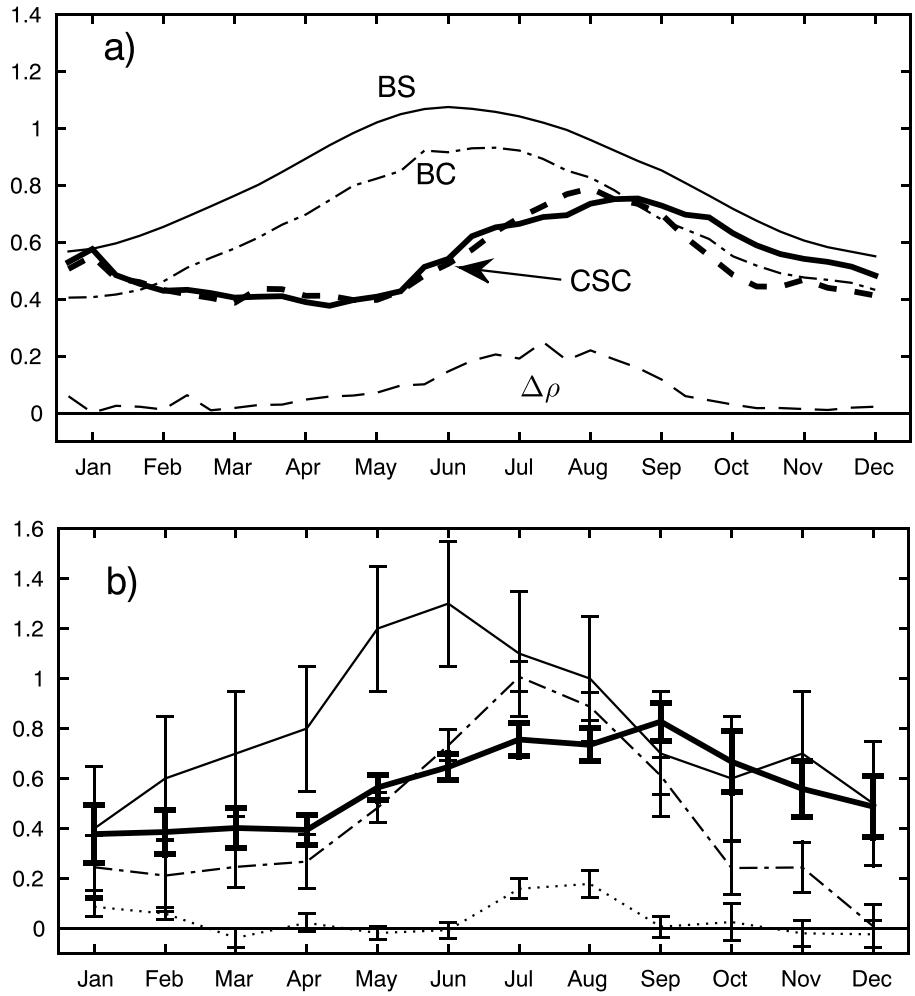

Figure 11. Seasonal mean time series of transports (Sv) from (a) the numerical model and (b) mooring observations. Bold solid lines: (a) westward transport between y = 1,100 km and y = 1,250 km for the model (indicative of the Chukchi Slope Current) and (b) based on the mooring array from 2013–2014. The bold dashed line in (a) is from the model runs with no seasonal cycle in Bering Strait velocity or wind and the full seasonal cycle in forcing of buoyancy at Bering Strait and surface heat flux. Thin solid lines: transport through Bering Strait (1990–2004 in b). Dash-dotted lines: transport through Barrow Canyon (2000–2008; 2010–2016). Dashed line in (a): difference in density between the surface and the bottom in Barrow Canyon for the full model run (kg/m^3). Dotted line in (b): eastward transport in Beaufort shelf break jet (2008–2012).

tion is that when the stratification is weak the flow is influenced more by the topography. This suggests that the Pacific water on the eastern flank of Barrow Canyon is more apt to follow the isobaths to the east into the Beaufort Sea. By contrast, a more strongly stratified current is less trapped by the bottom and more free to penetrate into the basin interior and turn toward the west. This interpretation is supported by the calculation with no seasonal cycle in wind or the velocity in Bering Strait to which the model is restored. The flow through Bering Strait and Barrow Canyon has only a weak seasonal cycle (not shown), but the westward transport in the Chukchi Slope Current displays nearly the same seasonal cycle as the standard calculation (bold dashed line).

With regard to the observed volume transports, we are constrained by the measurement periods and spatial coverage of the moorings. The biggest limitation is that while there exist climatological records for Bering Strait, Barrow Canyon, and the Beaufort shelf break jet, we have only a single year of data for the Chukchi Slope Current array, 2013–2014. Furthermore, the central Barrow Canyon mooring failed during 2013–2014, prohibiting a detailed comparison between the two sites for that year. Hence, the best we can do is consider a mix of climatology and the single-year record for the Chukchi slope site. We note that since the model forcing

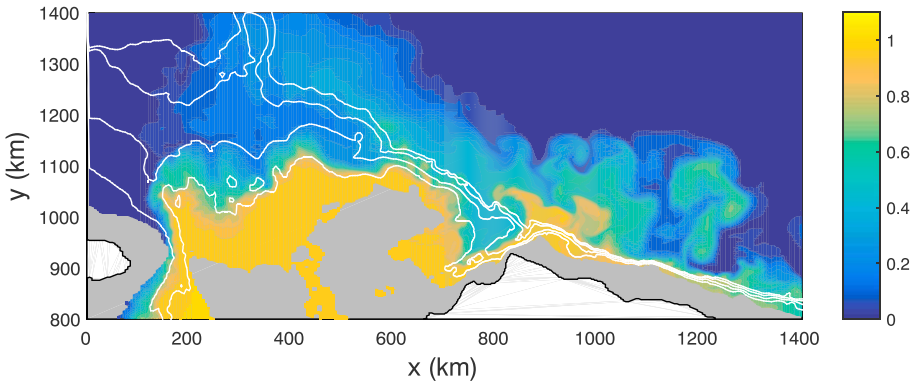

Figure 12. Pacific water tracer in the vicinity of the shelf break at 47.5-m depth at the end of year 2. The 60-, 100-, 200-, and 300-m isobaths are indicated by the white contours. Topography shallower than 47.5 m is shaded gray; land is white.

is derived from the Bering Strait climatology as published in Woodgate et al. (2005a), this is what we present for the Bering Strait observations.

Despite these shortcomings, there are encouraging similarities between the measured and modeled Pacific water transports (Figure 11b). In particular, Bering Strait and Barrow Canyon peak in June and July, respectively, although the seasonal cycle in the observations is stronger than that in the model (and the observed mean in Barrow Canyon is smaller than the model mean). Importantly, the peak in westward transport of the Chukchi Slope Current is 2–3 months later than this, consistent with the model. Furthermore, the slope current transport maximum occurs when the eastward transport of the Beaufort shelf break jet goes to zero in early fall. This supports the argument that a redirectioning of the flow out of Barrow Canyon is part of the reason for the seasonal timing of the slope current transport. Finally, we constructed a crude measure of the midwater column stratification in Barrow Canyon (centered at 60-m depth) using the mooring MicroCAT data, which reveals a peak in stratification in September/October, that is, later than transport peak in Barrow Canyon but close to the Chukchi Slope Current peak (not shown). This offers support for the notion that the lack of bottom trapping allows more of the outflow from Barrow Canyon to veer westward at this time of year. While there are disrecpancies between the model and data, the basic seasonality is similar in both.

4.4. Pacific Water Tracer

The exchange depicted in Figure 8 represents the source of Pacific origin waters to the halocline. The ventilation on the shelf and the pathways into the interior are diagnosed by consideration of two passive tracers in the model. The first marks Pacific origin waters advected into the Chukchi Sea within the forcing region in Bering Strait. It is given a value of 1 within the strait but is otherwise unforced outside of the strait. The second passive tracer is continuously set to 1 at the surface within the Chukchi Sea (isobath shallower than 60 m) and set to 0 below the surface layer within the forcing region in Bering Strait. This may be thought of as a ventilation tracer since it marks waters on the shelf that were within the mixed layer. Low values on the shelf indicate waters that were advected through Bering Strait but remained unventilated by contact with the surface layer.

A snapshot of the Pacific water tracer at 47.5-m depth near the shelf break at the end of the model calculation is shown in Figure 12. Areas shallower than 47.5 m are shaded gray. Over most of the region, the tracer remains shallower than the 100-m isobath. However, at and to the east of Barrow Canyon large amounts of shelf water are advected off-shelf. The primary injection site is along the eastern flank of Barrow Canyon, as indicated in Figure 8, although some plumes and eddies are seen forming farther to the east. (Note that eddies can flux tracers from the shelf to the interior but have no net volume flux.) The tracer breaks up into mesoscale eddies and filaments once in the interior and is transported both east and west from Barrow Canyon, consistent with the transport stream function in Figure 4. The weaker off-shelf flux near $x = 600$ km is the small outflow from Hanna Canyon. Importantly, there is a plume of Pacific water offshore of the 300-m isobath extending westward all the way to the Northwind Ridge, which is consistent with an eastern source and westward flow in the Chukchi Slope Current, rather than a local off-shelf flux west of $x = 600$ km.

The average of the Pacific water tracer as a function of distance from the 75-m isobath is shown in Figure 7d. There are two local maxima: one in the vicinity of the shelf break corresponding to the eastward flowing shelf break jet and the other centered near 80 km in the Chukchi Slope Current. The tracer concentration

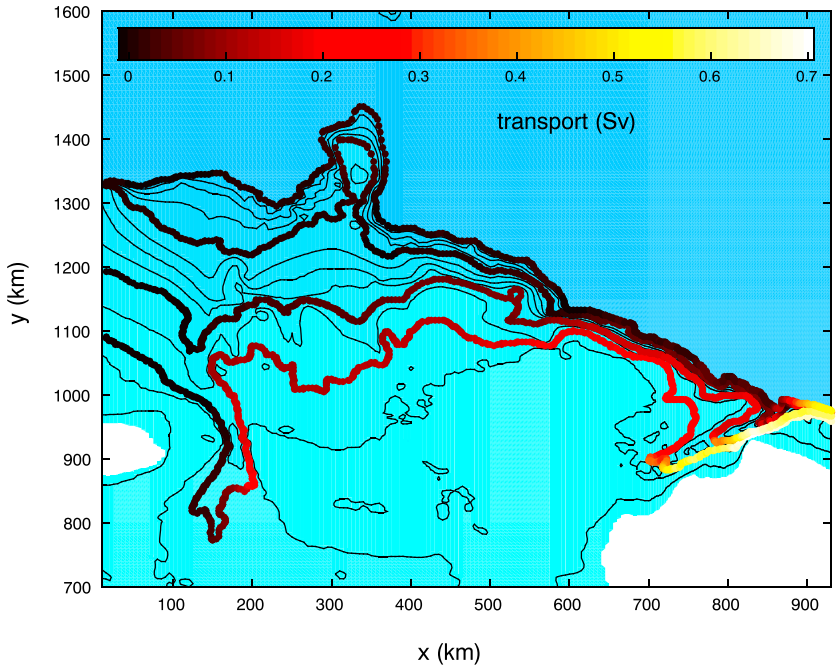

Figure 13. Cross-isobath transport (Sv) of Pacific water tracer along the 60-, 100-, 200-, and 300-m isobaths over the final year of integration. All start at 0 at the western boundary and integrate eastward along the topographic contours. Positive values indicate transport toward deeper water.

is a maximum around 100-m depth with lower concentrations near the surface. This directly connects the subsurface waters of the Chukchi Slope Current with the Barrow Canyon outflow. The tracer is smaller in the upper layer due to the influence of fresh water from ice melt getting mixed downward. This is consistent with the observations of Corlett and Pickart (2017). The resulting density structure supports a positive vertical shear, giving a maximum velocity near the surface, yet these waters did not predominantly come from Bering Strait in the 2-year period of integration, leading to the subsurface maximum in Pacific water tracer.

Evidence of where this off-shelf flux takes place is indicated by the total transport of Pacific water tracer across the 60-, 100-, 200-, and 300-m isobaths (Figure 13). The color of the bold lines represents the total transport of Pacific water tracer across each isobath, integrated from the surface to the bottom, starting from 0 at the western boundary. The regions of cross topography flux are indicated by a change in color from dark to light. The 60-m isobath has a large southward excursion in Herald Canyon, and we find about 0.2 Sv of cross topography flow within the canyon, with some of this returning to shallower water just east of the Canyon. From here, there is a more subtle increase toward the east, then an abrupt increase to 0.65 Sv within Barrow Canyon. Slightly deeper, at the 100-m isobath, there is only weak cross isobath transport west of $x = 600$ km, indicating that most of the transport across the 60-m isobath in Herald Canyon turns toward the east and remains onshore of the 100-m isobath. There is then a gradual increase to the east before another abrupt increase to 0.65 Sv within Barrow Canyon. The two deeper isobaths, 200 and 300 m, show very little cross isobath transport west of Barrow Canyon.

This total cross topography transport can be decomposed into mean and eddy contributions. We find that it is dominated by the mean flow, although the eddy transports are as large as 0.1 Sv within Barrow Canyon (Figure 14). There are also weaker off-shelf eddy fluxes between $x = 500$ km and Barrow Canyon, as suggested by Figure 12.

4.5. Extent of Ventilation on the Shelf

The Pacific water tracer indicates where these waters enter the basin interior but not where, or even if, these waters were ventilated within the Chukchi Sea. The product of the Pacific water tracer and the ventilation tracer is an indication of waters that flowed through Bering Strait and were ventilated or were within the surface mixed layer, within the Chukchi Sea. Unventilated Pacific water is the product of the Pacific water tracer and one minus the ventilation tracer. The volume of this unventilated water is shown in Figure 15 as a

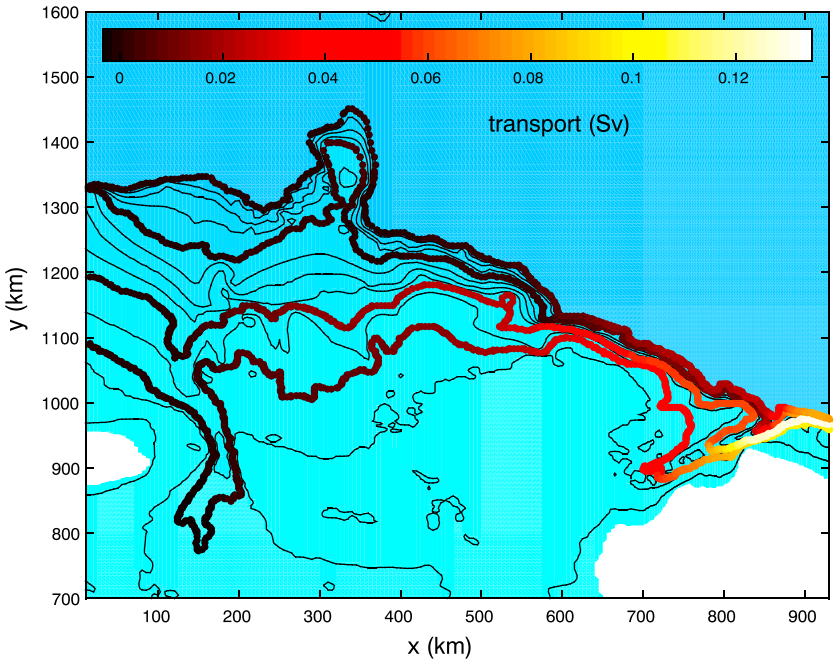

Figure 14. Cross-isobath eddy transport (Sv) of Pacific water tracer along the 60-, 100-, 200-, and 300-m isobaths over the final year of integration. All start at 0 at the western boundary and integrate eastward along the topographic contours. Positive values indicate transport toward deeper water.

function of time. The blue line is calculated over the region between the Bering Strait inflow and $y = 600$ km (i.e., south of Point Hope; see Figure 1). Initially there is none of this water because in winter the water column is well mixed throughout the southern Chukchi Sea. However, in late spring the flow through Bering Strait becomes stratified and unventilated water starts to be advected into the southern Chukchi Sea. This peaks in late summer, is rapidly reduced in fall, and is eliminated by the end of the year. This is a result of ice formation and brine rejection, which drives convective mixing to the bottom.

The green line is the same calculation for the region south of $y = 800$ km (roughly the latitude of Icy Cape, Figure 1). We find a similar temporal evolution but larger volume. This indicates that the unventilated water is advected beyond $y = 600$ km before winter sets in. The volume of unventilated water over the entire Chukchi shelf (red line), defined as everywhere shallower than 100 m, is larger still than that found south of $y = 800$ km. Importantly, some volume of this water remains between $y = 800$ km and the 100-m isobath all year round. In late fall the volume south of 800 km is reduced more rapidly than the volume shallower than 100 m. This indicates that the unventilated water is advected onto the outer Chukchi shelf, where it is at least partly shielded from convection. The volume of unventilated water at depth greater than 100 m steadily increases from the time the unventilated water first reaches the shelf break at 0.5 year until the end of the calculation (black line). The rate of increase corresponds to a mean cross topography flux of about 0.17 Sv and is nearly steady in time (i.e., no seasonal cycle). Recall that the mean Pacific water transport across the 100-m isobath is about 0.65 Sv, meaning that approximately 25% of the transport of Pacific water into the Canada Basin is not ventilated in the Chukchi Sea. The advective speeds through the Chukchi Sea are sufficiently fast that water parcels can transit the shelf before winter convection sets in. This differs from the subtropical gyres of the major ocean basins where the advective speeds are slow enough that only parcels that leave the mixed layer within a 1- or 2-month period at the end of winter are able to avoid getting entrained into the mixed layer in the following winter, thus resulting in a bias of the permanent thermocline properties toward those found at the end of winter in the mixed layer (Stommel, 1979; Williams et al., 1995).

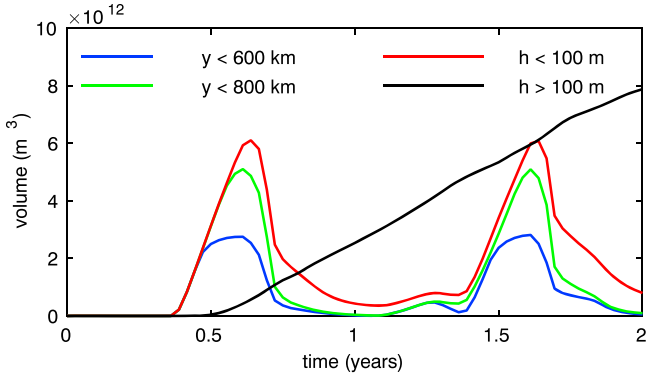

Figure 15. Volume of unventilated Pacific water within various regions of the Chukchi shelf and interior. Blue: south of $y = 600$ km. Green: south of $y = 800$ km. Red: shallower than 100 m. Black: deeper than 100 m.

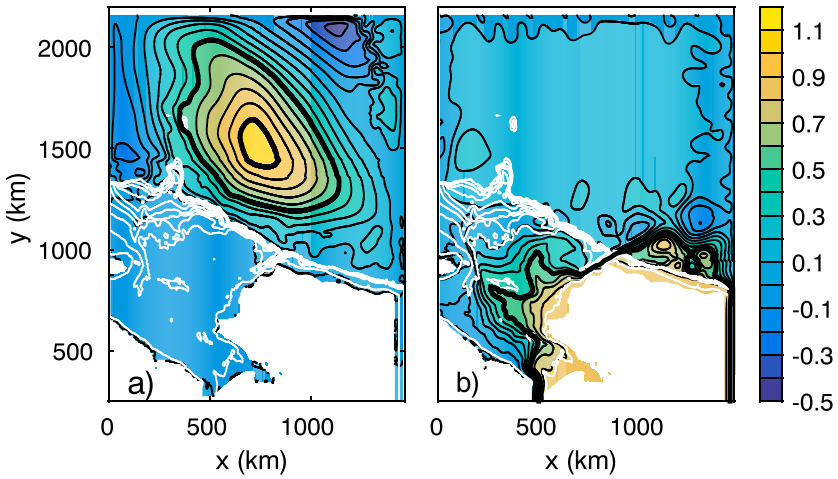

Figure 16. Mean upper ocean transport stream function (surface to 300 m) over the 2-year integrations for (a) case with atmospheric forcing and a closed Bering Strait and (b) forcing in Bering Strait but with no atmospheric forcing.

4.6. Relation to the Beaufort Gyre

It is instructive to consider the relationship between the Chukchi Slope Current and the Beaufort Gyre. The flow is westward and surface intensified for both features; however, there are important differences. To the extent that the circulation dynamics in the basin interior are linear, we may consider the fully forced problem as the sum of the wind- and buoyancy-forced interior circulation and the circulation that results from the flow through Bering Strait in the absence of any atmospheric forcing. The model run identical to the fully forced case but with a closed Bering Strait (model run no-inflow) produces an anticyclonic Beaufort Gyre (Figure 16a) much as is found in the fully forced case. The primary difference in the basin interior is that, in the absence of Bering Strait inflow, there is westward flow offshore of the Beaufort slope, to the east of Barrow Canyon (900km $< x <$ 1,300 km), whereas the fully forced circulation shows weak eastward flow. The case with only flow through Bering Strait (model run no-atmos, Figure 16b) produces the three main branches flowing through the Chukchi Sea and a strong transport through Barrow Canyon (the flow through the Chukchi Sea is shifted to the east in the fully forced case as a result of the cyclonic wind stress curl (Spall, 2007)). The flow exits Barrow Canyon, and most of it crosses the isobaths, penetrates into the southern part of the basin, and turns to the east before exiting the domain.

If the flow were purely linear, the sum of these two solutions would be equal to the solution for the fully forced case. While the model is not linear, we can see that the tendency of adding these solutions together is to produce a large-scale circulation that resembles the fully forced case. Off the Beaufort shelf the eastward transport of the Bering Strait case will diminish the westward transport of the wind-driven gyre, particularly nearer the coast, resulting in only weak westward or even eastward flow. This is largely what we find for the fully forced calculation. This is also true of the observations: there is weak eastward flow offshore of the Beaufort shelf break jet at least out to the 700-m isobath (Figure 6b; see also Nikolopoulos et al., 2009). To the west of Barrow Canyon, the Bering Strait forced case produces no flow, so the linear sum would have the same westward transport as the Beaufort Gyre case, which is also consistent with the fully forced model result. However, the source of this westward flow is Barrow Canyon, not a recirculation of the Beaufort Gyre water from the east.

The linear sum is useful for understanding the pressure field but it does not directly apply to the tracer field. The Chukchi Slope Current is a well-defined feature in the full model with an offshore edge that is distinguishable from the southern portion of the Beaufort Gyre (Figure 7). This most likely relates to the distinct core of Pacific water (Figure 7c and Figures 4 and 5 of Corlett & Pickart, 2017), which will alter the velocity profile through the thermal wind balance. Also, as seen above, the seasonal variability of the westward transport appears to originate from the Chukchi Sea in the model as well as the observations; that is, it is not an inherent part of the wind-driven Beaufort Gyre.

5. Summary and Discussion

The primary objective of this study was to understand where and how Pacific waters exit the Chukchi shelf and how this relates to the formation of the Chukchi Slope Current. This process is essential for maintenance of the halocline, providing nutrients and zooplankton to the local ecosystem, and insulation of sea ice from the warm Atlantic Waters below. It has long been known that Pacific waters get modified on the Chukchi shelf and enter the basin interior, but the means by which this occurs is not well understood.

The primary pathway in a high-resolution regional ocean/ice model was shown to be nonlinear advection through Barrow Canyon. The transports in the model Chukchi Sea and at three key locations — Barrow Canyon, the Beaufort shelf break, and the Chukchi shelf break and slope — are consistent with observational estimates, providing confidence in the utility of the model fields. After crossing the topography in Barrow Canyon, most of the transport turns to the west and forms the Chukchi Slope Current. Similar cross-shelf flow and westward transport have been previously found in numerical models (Aksenov et al., 2016; Timmermans et al., 2014; Watanabe et al., 2017; Zhang et al., 2016), but their focus was not on this process and its role in providing source waters to the halocline. We consider this transport to have replaced Beaufort Gyre water that would have been advected from the east in the absence of the flow out of Barrow Canyon. Our finding, in both observations and the model, that the flow east of Barrow Canyon and offshore of the shelf break is weakly toward the east supports this interpretation. Dynamically, one can think of this circulation as the linear sum of the wind-driven anticyclonic gyre and the cross-topography flow exiting Barrow Canyon that ultimately is driven by flow through Bering Strait. While the westward flow is balanced by the the sea surface height slope and the anticyclonic wind stress curl, as is the Beaufort Gyre, the source region and water mass properties are different from the large-scale Beaufort Gyre circulation and so we consider this a distinct current.

This advective process is operative at all times of year, although the peak westward transport in the Chukchi Slope Current occurs in late summer, several months later than the peak transport through Bering Strait. The delay appears to be related to stronger stratification, weaker topographic control, and more off-shelf transport at the end of summer. Although we lack a simple theoretical model, the basic mechanism here is nonlinear advection as a result of topographic steering on the shelf guiding the flow into the narrow Barrow Canyon. Based on the model calculations and a linear vorticity scaling, we conclude that wind forcing plays no role in this process. We find no evidence for wind-driven exchange broadly distributed along the shelf break, analogous to the midlatitude subtropical gyre subduction process, as proposed by Timmermans et al. (2014, 2017). This is likely due to a combination of the very strong topographic beta, which minimizes the ocean response to Ekman pumping, and the moderation of stress transmitted to the ocean current because of the seasonally concentrated sea ice cover (Meneghello et al., 2018).

Acknowledgments
This study was supported by the National Science Foundation under grants PLR-1415489 and OCE-1533170 (M. A. S.), the Bureau of Ocean and Energy Management under contract M12AC00008 (R. S. P. and M. L.), the National Natural Science Foundation of China (grant 41506018) and the Project of Enhancing School with Innovation of Guangdong University (M. L.), and the National Oceanic and Atmospheric Administration grant NA16OAR4310248 (P. L.). The Barrow Canyon mooring works were supported by JAMSTEC Arctic Research and Japan's research project, Arctic Challenge for Sustainability (ArCS), which was funded by the Ministry of Education, Culture, Sports, Science, and Technology of Japan (MEXT). The authors would like to thank two anonymous reviewers for their helpful comments and suggestions for improving this manuscript. Data from the Beaufort slope array are available at http://aon.whoi.edu. The Chukchi slope mooring data are available through the Bureau of Ocean and Energy Management (https://www.boem.gov). The Chukchi slope hydrographic and shipboard ADCP data are available through http://hdl.handle.net/1912/8170. The Barrow Canyon mooring data can be found at http://www.jamstec.go.jp/arctic/data_archive_work/mooring/mooring_index.html. The Bering Strait mooring data are available at http://psc.apl.washington.edu/HLD/Bstrait/Data/BeringStraitMooringDataArchive.html. The numerical model input parameters, forcing fields, and configuration are available at the NSF Arctic Data Center, https://arcticdata.io/catalog/\#view/doi:10.18739/A21C4S.

References

Aksenov, Y., Karcher, M., Proshutinsky, A., Gerdes, R., de Cuevas, B., Golubeva, E., et al. (2016). Arctic pathways of Pacific water: Arctic Ocean Model Intercomparison experiments. *Journal of Geophysical Research: Oceans*, *121*, 27–59. https://doi.org/10.1002/2015JC011299

Ashjian, C. J., Braund, S. R., Campbell, R. G., George, J. C., Kruse, J., Maslowski, W., et al. (2010). Climate variability, oceanography, bowhead whale distribution, and Iñupiat subsistence whaling near Barrow, Alaska. *Arctic*, *63*(2), 179–194.

Brugler, E. T., Pickart, R. S., Moore, G. W. K., Roberts, S., Weingartner, T. J., & Statscewich, H. (2014). Seasonal to interannual variability of the Pacific water boundary current in the Beaufort Sea. *Progress in Oceanography*, *127*, 1–20.

Codispoti, L. A., Flagg, C., Kelly, V., & Swift, J. H. (2005). Hydrographic conditions during the 2002 SBI process experiments. *Deep-Sea Research Part II*, *52*, 3199–3226.

Corlett, W. B., & Pickart, R. S. (2017). The Chukchi slope current. *Progress in Oceanography*, *153*, 50–65.

Cross, J., Mathis, J., Pickart, R. S., & Bates, N. (2017). Formation and transport of corrosive water in the Pacific Arctic region. *Deep-Sea Research Part II*, *152*, 76–81.

Gong, D., & Pickart, R. S. (2015). Summertime circulation in the eastern Chukchi Sea. *Deep-Sea Research Part II: Topical Studies in Oceanography*, *118*, 18–31.

Hopcroft, R. R., Kosobokova, K. N., & Pinchuk, A. I. (2010). Zooplankton community patterns in the Chukchi Sea during summer 2004. *Deep Sea Research Part II: Topical Studies in Oceanography*, *57*(1-2), 27–39.

Hunke, E. C., & Dukowicz, J. K. (1997). An elastic-viscous-plastic model for sea ice dynamics. *Journal of Physical Oceanography*, *27*, 1849–1867.

Itoh, M., Nishino, S., Kawaguchi, Y., & Kikuchi, T. (2013). Barrow Canyon volume, heat, and freshwater fluxes revealed by long-term mooring observations between 2000 and 2008. *Journal of Geophysical Research: Oceans*, *118*, 4363–4379. https://doi.org/10.1002/jgrc.20290

Jackett, D. R., & McDougall, T. J. (1995). Minimal adjustment of hydrographic profiles to achieve static stability. *Journal of Atmospheric and Oceanic Technology*, *12*, 381–389.

Large, W. G., McWilliams, J. C., & Doney, S. C. (1994). Oceanic vertical mixing: A review and a model with a nonlocal boundary layer parameterization. *Reviews of Geophysics*, *32*, 363–403.

Large, W. G., & Pond, S. (1981). Open ocean momentum flux measurements in moderate to strong winds. *Journal of Physical Oceanography*, *11*, 324–336.

Li, M., & Pickart, R. S. (2017). Circulation of the Chukchi Sea shelfbreak and slope from moored timeseries. Abstract presented at 2017 Alaska Marine Symposium, NPRB, Anchorage, AK.
Manley, T. O., & Hunkins, K. (1985). Mesoscale eddies of the Arctic Ocean. *Journal of Geophysical Research*, *90*, 4911–4930.
Marshall, J., Hill, C., Perelman, L., & Adcroft, A. (1997). Hydrostatic, quasi-hydrostatic, and non-hydrostatic ocean modeling. *Journal of Geophysical Research*, *102*, 5733–5752.
Mathis, J. T., Pickart, R. S., Hansell, D. A., Kadko, D., & Bates, N. R. (2007). Eddy transport of organic carbon and nutrients from the Chukchi shelf into the deep Arctic basin, *112*, CO5011.
Meneghello, G., Marshall, J., Timmermans, M.-L., & Scott, J. (2018). Observations of seasonal upwelling and downwelling in the Beaufort Sea mediated by sea ice. *Journal of Physical Oceanography*, *48*, 795–805.
Mizobata, K., Watanabe, E., & Kimura, N. (2016). Wintertime variability of the Beaufort Gyre in the Arctic Ocean derived from CryoSat-2/SIRAL observations. *Journal of Geophysical Research: Oceans*, *121*, 1685–1699. https://doi.org/10.1002/2015JC011218
Moore, G. W. K. (2012). Decadal variability and a recent amplification of the summer Beaufort Sea high. *Geophysical Research Letters*, *39*, L10807. https://doi.org/10.1029/2012GL051570
Nelson, R. J., Carmack, E. C., McLaughlin, F. A., & Cooper, G. A. (2009). Penetration of Pacific zooplankton into the western Arctic Ocean tracked with molecular population genetics. *Marine Ecology Progress Series*, *381*, 129–138.
Nikolopoulos, A., Pickart, R. S., Fratantoni, P. S., Shimada, K., Torres, D. J., & Jones, E. P. (2009). The western Arctic boundary current at 152°W: Structure, variability, and transport. *Deep-Sea Research II*, *56*, 1164–1181.
Panteleev, G., Nechaev, D. A., Proshutinsky, A., Woodgate, R., & Zhang, J. (2010). Reconstruction and analysis of the Chukchi Sea circulation in 1990–1991. *Journal of Geophysical Research*, *115*, 1–22. https://doi.org/10.1029/2009JC005453
Paquette, R. G., & Bourke, R. H. (1974). Observations on the coastal current of Arctic Alaska. *Journal of Marine Research*, *32*(2), 195–207.
Pickart, R. S., Moore, G. W. K., Mao, C., Bahr, F., Nobre, C., & Weingartner, T. J. (2016). Circulation of winter water on the Chukchi shelf in early summer. *Deep-Sea Research Part II: Topical Studies in Oceanography*, *130*, 56–75.
Pickart, R. S., Pratt, L. J., Torres, D. J., Whitledge, T. E., Proshutinsky, A. Y., Aagaard, K., et al. (2010). Evolution and dynamics of the flow through Herald Canyon in the western Chukchi Sea. *Deep-Sea Research II*, *57*, 5–26.
Pickart, R. S., Spall, M. A., Moore, G. W. K., Weingartner, T. J., Woodgate, R. A., Aagaard, K., & Shimada, K. (2011). Upwelling in the Alaskan Beaufort Sea: Atmospheric forcing and local versus non-local response. *Progress in Oceanography*, *88*, 78–100.
Pickart, R. S., & Stossmeister, G. (2009). Outflow of water from the Chukchi Sea to the Arctic Ocean. *Chinese Journal of Polar Science*, *9*, 135–148.
Pickart, R. S., Weingartner, T. J., Zimmermann, S., Torres, D. J., & Pratt, L. J. (2005). Flow of winter-transformed Pacific water into the western Arctic. *Deep-Sea Research Part II*, *52*, 3175–3198.
Proshutinsky, A., Bourke, R. H., & McLaughlin, F. A. (2002). The role of the Beaufort Gyre in Arctic climate variability: Seasonal to decadal climate scales. *Geophysical Research Letters*, *29*(23), 2100. https://doi.org/10.1029/2002GL015847
Proshutinsky, A., Dukhovskoy, D., Timmermans, M.-L., Krishfield, R., Bamber, J. L., & Proshutinsky, A. (2015). Arctic circulation regimes. *Philosophical Transactions of the Royal Society A*, *373*, 20140160.
Proshutinsky, A, Krishfield, R, Timmermans, M. L., Toole, J., Carmack, E., McLaughlin, F., et al. (2009). Beaufort Gyre freshwater reservoir: State and variability from observations. *Journal of Geophysical Research*, *114*, C00A1. https://doi.org/10.1029/2008JC005104
Semtner, A. J. (1976). A model for the thermodynamic growth of sea ice in numerical investigations of climate. *Journal of Physical Oceanography*, *6*, 379–389.
Smagorinsky, J. (1963). General circulation experiments with the primitive equations: I. The basic experiment. *Monthly Weather Review*, *91*, 99–164.
Spall, M. A. (2007). Circulation and water mass transformation in a model of the Chukchi Sea. *Journal of Geophysical Research*, *112*, C05025. https://doi.org/10.1029/2005JC003364
Spall, M. A., Pickart, R. S., Fratantoni, P. S., & Plueddemann, A. J. (2008). Western Arctic shelfbreak eddies: Formation and transport. *Journal of Physical Oceanography*, *38*, 1644–1668.
Stabeno, P., Kachel, N., Ladd, C., & Woodgate, R. (2018). Flow patterns in the eastern Chukchi Sea: 2010–2015. *Journal of Geophysical Research: Oceans*, *123*, 1177–1195. https://doi.org/10.1002/2017JC013135
Steele, M., Morley, R., & Ermold, W. (2001). PHC: A global ocean hydrography with a high quality Arctic Ocean. *Journal of Climate*, *14*, 2079–2087.
Stommel, H. (1979). Determination of watermass properties of water pumped down from the Ekman layer to the geostrophic flow below. *Proceedings of the National Academy of Sciences of the United States of America*, *76*, 3051–3055.
Timmermans, M.-L., Marshall, J., Proshutinsky, A., & Scott, J. (2017). Seasonally derived components of the Canada Basin halocline. *Geophysical Research Letters*, *44*, 5008–5015. https://doi.org/10.1002/2017GL073042
Timmermans, M.-L., Proshutinsky, A., Golubeva, E., Jackson, J. M., Krishfield, R., McCall, M., et al. (2014). Mechanisms of Pacfic summer water variability in the Arctic's Central Canada Basin. *Journal of Geophysical Research: Oceans*, *119*, 7523–7548. https://doi.org/10.1002/2014JC010273
Wassmann, P., Kosobokova, K. N., Slagstad, D., Drinkwater, K. F., Hopcroft, R. R., Moore, S. E., et al. (2015). The contiguous domains of Arctic Ocean advection: Trails of life and death. *Progress in Oceanography*, *139*, 42–65.
Watanabe, E., Onodero, J., Itoh, M., Nishino, S., & Kikuchi, T. (2017). Winter transport of subsurface warm water toward the Arctic Chukchi Borderland. *Deep-Sea Research Part I*, *128*, 115–130.
Weingartner, T. J., Aagaard, K., Woodgate, R., Danielson, S., Sasaki, Y., & Cavalieri, D. (2005). Circulation on the north central Chukchi shelf. *Deep Sea Research II*, *52*, 3150–3174.
Weingartner, T. J., Irvine, C., Dobbins, E., Danielson, S., DeSousa, L., Adams, B., et al. (2015). Satellite-tracked drifter measurements in the Chukchi and Beaufort Seas (*Technical Report 2015-022*). Anchorage: Bureau of Ocean Energy Management. http://www.boem.gov/BOEM-2015-022
Weingartner, T. J., Potter, R., Stoudt, C. A., Dobbins, E. L., Statscewich, H., Winsor, P. R., et al. (2017). Transport and thermohaline variability in Barrow Canyon on the northeastern Chukchi shelf. *Journal of Geophysical Research: Oceans*, *122*, 2017–2033. https://doi.org/10.1002/2016JC012636
Williams, R. G., Spall, M. A., & Marshall, J. C. (1995). Does Stommel's mixed-layer 'demon' work? *Journal of Physical Oceanography*, *25*, 3089–3102.
Winsor, P., & Chapman, D. C. (2004). Pathways of Pacific water across the Chukchi Sea: A numerical model study. *Journal of Geophysical Research*, *109*, C03002. https://doi.org/10.1029/2003JC001962
Winton, M. (2000). A reformulated three-layer sea ice model. *Journal of Atmospheric and Oceanic Technology*, *17*, 525–531.

Woodgate, R. A. (2017). Increases in the Pacific inflow to the Arctic from 1990 to 2015, and insights into seasonal trends and driving mechanisms from year-round Bering Strait mooring data. *Progress in Oceanography*, *160*, 124–154.

Woodgate, R. A., Aagaard, K., & Weingartner, T. (2005a). Monthly temperature, salinity, and transport variability in the Bering Strait through flow. *Geophysical Research Letters*, *32*, L04601. https://doi.org/10.1029/2004GL021880

Woodgate, R. A., Aagaard, K., & Weingartner, T. (2005b). A year in the physical oceanography of the Chukchi Sea. *Deep-Sea Research Part II*, *52*, 3116–3149.

Woodgate, R. A., Weingartner, T. J., & Lindsay, R. (2012). Observed increases in Bering Strait oceanic fluxes from the Pacific to the Arctic from 2001 to 2011 and their impacts on the Arctic Ocean water column. *Geophysical Research Letters*, *39*, L24603. https://doi.org/10.1029/2012GL054092

Zhang, J., Steele, M., Runciman, K., Dewey, S., Morison, J., Lee, C., et al. (2016). The Beaufort Gyre intensification and stabilization: A model-observation synthesis. *Journal of Geophysical Research: Oceans*, *121*, 7933–7952. https://doi.org/10.1002/2016JC012196

Zhao, M., Timmermans, M.-L., Cole, S., Krishfield, R., Proshutinsky, A., & Toole, J. (2014). Characterizing the eddy field in the Arctic Ocean. *Journal of Geophysical Research: Oceans*, *119*, 8800–8817. https://doi.org/10.1002/2014JC010488